

SOLAR ABUNDANCES FROM GAMMA-RAY SPECTROSCOPY: COMPARISONS WITH ENERGETIC PARTICLE, PHOTOSPHERIC, AND CORONAL ABUNDANCES

R. J. MURPHY

Universities Space Research Association, Goddard Space Flight Center¹

R. RAMATY

Code 665, Laboratory for High Energy Astrophysics, Goddard Space Flight Center, Greenbelt, MD 20771

B. KOZLOVSKY

Raymond and Beverly Sackler Faculty of Exact Sciences, School of Physics and Astronomy, Tel Aviv University, Ramat Aviv, Tel Aviv, Israel

AND

D. V. REAMES

Code 661, Laboratory for High Energy Astrophysics, Goddard Space Flight Center, Greenbelt, MD 20771

Received 1990 April 18; accepted 1990 October 1

ABSTRACT

We have derived accelerated particle and ambient gas abundances using solar flare gamma-ray spectroscopy. We compare the results with photospheric and coronal abundances, as well as with solar energetic particle abundances. This is the first time that the composition of accelerated particles interacting in an astrophysical source has been compared with the composition of particles escaping from the source. Our analysis shows that the derived composition of the accelerated particles is different from the composition of particles observed in large proton flares; rather, it resembles the composition observed in ³He-rich flares. Our analysis also suggests an ambient gas composition which differs from the composition of both the photosphere and the corona.

Subject headings: gamma rays: general — Sun: abundances — Sun: flares — Sun: particle emission

1. INTRODUCTION

The compositions of the various regions of the solar atmosphere have been studied using atomic and molecular spectroscopy, and solar wind and solar energetic particle (SEP) observations (e.g., Anders & Grevesse 1989). These studies have revealed considerable abundance variations. In particular, the SEP composition was found to be highly variable, changing from flare to flare and with time and energy within a flare. It has been shown (Reames 1990) that enhanced abundances of ³He relative to ⁴He and of elements heavier than O relative to C distinguish a first class of SEP events from a second class consisting of events with lower values of ³He/⁴He and lower ratios of heavy elements to C. Based on the temperatures derived from the observed charge states of Fe ions in SEP events (Luhn et al. 1987), it has been suggested (Lin 1987) that particles in first-class events are accelerated from hot (10⁷ K) flare plasma, and that those in second-class events are accelerated from the quiescent corona. Such hot plasma is known to exist in solar flare magnetic loops. First-class events are often referred to as ³He-rich events; because second-class events exhibit large proton fluxes, they are referred to as large proton events. The observed SEP composition of large proton events has been used to derive the composition of the corona (Meyer 1985; Breneman & Stone 1985). Based on such SEP data and other data it has been shown that the coronal abundances of heavy elements with high first ionization potential (FIP) are reduced relative to those with lower FIP, as compared to photospheric abundances (e.g., Meyer 1985).

Information on solar abundances has also been obtained from nuclear gamma-ray spectroscopy (Murphy et al. 1985a,

b). The principal mechanisms for the production of gamma-ray lines are nuclear de-excitation, neutron capture, and positron annihilation (e.g., Ramaty, Kozlovsky, & Lingenfelter 1975; 1979). Nuclear de-excitation lines result from the bombardment of ambient gas with accelerated protons, α -particles, and ³He nuclei, and from the inverse reactions in which ambient hydrogen and helium are bombarded by accelerated C and heavier nuclei. The former lead to narrow lines whose widths are determined by the recoil velocities of the heavy targets, while the latter produce broad lines whose widths are due to the velocities of the accelerated heavy projectiles. The strengths of the narrow lines depend primarily on the ambient gas abundances, while the strengths of the broad lines depend primarily on the accelerated particle abundances.

The bulk of the observed gamma-ray emission from solar flares is thought to be produced by particles accelerated and trapped in closed loops (Ramaty & Murphy 1987). This is based on the comparison of the number of protons that escape from the flare (from SEP observations) with the number that remain and interact at the Sun (from gamma-ray line observations of the same flare), showing that the interacting protons are generally more numerous than the escaping ones. Within these loops, the acceleration probably takes place in the coronal portions, but the nuclear reactions may occur at various depths (e.g., Ramaty et al. 1990). It has been shown (Hua, Ramaty, & Lingenfelter 1989) that, for flares for which the decay times of the observed nuclear de-excitation gamma-ray emission are short (e.g., the 1980 June 21 flare), these reactions probably occur in the chromospheric and photospheric portions of the loops. However, for flares with longer decay times (such as the 1981 April 27 flare which we treat below), a significant fraction of the reactions may occur in the corona.

The first attempt to deduce abundances from solar flare

¹ Current postal address: E. O. Hulburt Center for Astrophysics, Code 4154, Naval Research Laboratory, Washington, DC 20375.

gamma-ray observations was made by Ramaty et al. (1980). It was shown that a feature between 1 and 2 MeV in the spectrum of the 1972 August 4 flare, observed with a low-resolution gamma-ray spectrometer on *OSO 7* (Suri et al. 1975), could be due to the broad de-excitation lines resulting from interactions of accelerated particles with enhanced Ne/C, Mg/C, Si/C, and Fe/C relative to the corresponding abundance ratios in the photosphere or in large proton flares. However, the narrow Ne, Mg, Si, and Fe de-excitation lines that are also expected in the 1–2 MeV range could not be discerned in these 1972 August 4 observations. These narrow lines were subsequently observed with the gamma-ray spectrometer on *SMM* from many flares. Using the *SMM* data for the 1981 April 27 flare, Forrest (1983) showed that a theoretically calculated gamma-ray spectrum (Ramaty, Kozlovsky, & Lingenfelter 1979) for which both the ambient gas and the accelerated particles have photospheric composition provides an unacceptable fit to the data, but that a better fit would result from a spectrum obtained by enhancing the abundances of ambient Ne, Mg, Si, and Fe relative to C and O. Using the same data, Murphy et al. (1985a, b) derived the best-fitting ambient gas abundances. In this study the accelerated particle abundances were held fixed at large proton flare (LPF) values, and the ambient abundances were varied until a best fit to the data was obtained. The results suggested that ambient Mg/C, Si/C, and Fe/C are enhanced relative to the corresponding photospheric ratios but are consistent with the coronal values; that Ne/C and Ne/O are larger than the coronal values; and that O/C is consistent with both the photospheric and coronal values. However, it has since been shown (Murphy et al. 1990b) that the derived strengths of the narrow lines are sensitive to the underlying continuum to which the board lines make a significant contribution, raising the question whether accurate ambient gas abundances can be obtained with fixed accelerated particle abundances.

In the present paper we relax the constraint that the accelerated particle composition is fixed, and we show that the *SMM* gamma-ray data are of sufficient resolution to allow the determination of the abundances of both these particles and the ambient gas. We use a numerical code which incorporates the most recent accelerator cross section measurements to calculate nuclear de-excitation spectra for a wide range of parameters, and we describe in detail how these calculations are used to derive the abundances. We compare the results to photospheric and coronal abundances, as well as to SEP abundances in both ³He-rich flares and large proton flares. This is the first time that the composition of accelerated particles interacting in an astrophysical source is compared with the composition of the particles escaping from the source. In § 2 we present the gamma-ray spectral analysis, and we compare the results for the composition of the ambient medium with photospheric and coronal compositions. In § 3 we compare the results for the composition of the accelerated particles to SEP observations, and we summarize our results in § 4.

2. GAMMA-RAY SPECTRAL ANALYSIS

Nuclear cross sections, obtained from accelerator measurements, and the relevant nuclear kinematics were incorporated (Ramaty, Kozlovsky, & Lingenfelter 1979; Murphy 1985) into a computer code which produces a complete de-excitation gamma-ray spectrum for a given accelerated particle spectrum and given compositions of both the accelerated particles and the ambient medium. We have updated this code using new,

accurately measured cross sections and will publish the details elsewhere. The strongest nuclear de-excitation lines are at 6.129 MeV from ¹⁶O, 4.438 MeV from ¹²C, 1.779 MeV from ²⁸Si, 1.634 MeV from ²⁰Ne, 1.369 MeV from ²⁴Mg, 0.847 MeV from ⁵⁶Fe, 0.478 MeV from ⁷Li, and 0.429 MeV from ⁷Be. There are also strong lines from neutron capture at 2.223 MeV and positron annihilation at 0.511 MeV. All of these lines are superposed on a continuum due to bremsstrahlung of accelerated electrons.

We construct a theoretical gamma-ray spectrum from a nuclear de-excitation spectrum calculated by using an isotropic thick-target model, to which we add the very narrow lines at 2.223 and 0.511 MeV, the bremsstrahlung continuum, and a continuum due to orthopositronium annihilation (Cranell et al. 1976; Ramaty & Murphy 1987). We assume that Compton scattering at the Sun is negligible (except for the attenuation of the 2.223 MeV line), that the bremsstrahlung continuum can be approximated by a power law, and that the orthopositronium continuum corresponds to a positronium fraction of 2/3 (Murphy et al. 1990a). We also assume that all of the accelerated particle species have the same energy spectrum as a function of energy per nucleon and that this spectrum is given by the modified Bessel function characterized by the parameter αT appropriate for stochastic acceleration (Forman, Ramaty, & Zweibel 1986).

Such a theoretical spectrum depends on 23 parameters: 16 abundances (ambient ⁴He, N, O, Ne, Mg, Si, and Fe relative to C; ambient ⁴He relative to H, [⁴He/¹H]_{amb}; accelerated ³He relative to ⁴He; accelerated N, O, Ne, Mg, Si, and Fe relative to C; accelerated α -particles relative to protons, [⁴He/¹H]_{acc}); two normalizations ($[n_C/n_H]N_p$ and N_C , where N_p and N_C are the total numbers of accelerated protons and C nuclei of energies greater than 30 MeV/nucleon incident on the thick target, and n_C/n_H is the ambient C-to-H abundance ratio); the 2.223 and 0.511 MeV line fluxes; the amplitude and spectral index s of the bremsstrahlung power law; and the spectral parameter αT of the accelerated particles. However, since we find that the results are essentially independent of [⁴He/¹H]_{amb}, we have fixed this parameter at the photospheric value of 0.1 (Anders & Grevesse 1989), thereby reducing the number of free parameters to 22. The calculated gamma-ray spectrum depends linearly on these parameters, except s , αT , and [⁴He/¹H]_{acc}. We consider five cases (Table 1): in case 1, all 22 parameters are allowed to vary; in cases 2 and 3, the ambient abundances are fixed at photospheric and coronal values, respectively (Anders & Grevesse 1989); in case 4, the accelerated particle abundances (except [⁴He/¹H]_{acc} and [³He/⁴He]_{acc}) are fixed at the average values for large proton flares (Breneman & Stone

TABLE 1
ANALYSIS CASES AND ASSOCIATED QUALITIES OF FIT

Case	χ^2	ν	P_{χ^2}
1. Full fit	459.2	427	0.136
2. Fixed ambient abundances ^a	484.0	434	0.049
3. Fixed ambient abundances ^b	487.6	434	0.038
4. Fixed accelerated particle abundances ^c	477.5	433	0.069
5. Fixed ambient ^a and accelerated ^c particle abundances	990.9	439	<10 ⁻⁶

^a Photospheric (Anders & Grevesse 1989).

^b Coronal (Breneman & Stone 1985).

^c Large proton flare (LPF) (Breneman & Stone 1985).

1985); and in case 5, both the ambient and accelerated particle abundances (except $[\text{}^4\text{He}/\text{C}]_{\text{amb}}$, $[\text{}^4\text{He}/\text{}^1\text{H}]_{\text{acc}}$, and $[\text{}^3\text{He}/\text{}^4\text{He}]_{\text{acc}}$) are fixed at photospheric (Anders & Grevesse 1989) and LPF abundances, respectively.

We compare data (Murphy et al. 1990b) from the 1981 April 27 flare, obtained with the *SMM* gamma-ray spectrometer, with theoretical spectra folded through the response function of this detector. These data are given in 449 pulse-height channels ranging from 0.3 to 8.5 MeV. We measure the quality of fit with a statistic which differs from χ^2 only in that uncertainties in the channel counts are estimated from the data rather than from the model. Therefore, this statistic should be distributed similarly to χ^2 , and thus, for simplicity, we refer to it as χ^2 (see Murphy et al. 1990a). Associated with χ^2 is P_{χ^2} , the probability that random observations of the actual solar spectrum would produce a χ^2 as large or larger than the one obtained with the model. It has been shown (Trombka & Schmadebeck 1968; Murphy 1985) that, for a given choice of s , αT , and $[\text{}^4\text{He}/\text{}^1\text{H}]_{\text{acc}}$, χ^2 can be minimized by matrix inversion, leading to the best-fitting values of the other parameters. The minimal χ^2 (and the maximal P_{χ^2}) can then be obtained by a systematic search in the three-dimensional s - αT - $[\text{}^4\text{He}/\text{}^1\text{H}]_{\text{acc}}$ parameter space.

For cases 1 through 4 we show in Figures 1a–1d, respectively, P_{χ^2} as a function of $[\text{}^4\text{He}/\text{}^1\text{H}]_{\text{acc}}$ for various values of αT . Along each of these curves all other parameters have been

adjusted to minimize χ^2 . The absolute maximal P_{χ^2} values, the corresponding χ^2 values, and the numbers of degrees of freedom ν are given in Table 1, except for case 5. In this case, the given values correspond only to the maximal P_{χ^2} achieved (at $[\text{}^4\text{He}/\text{}^1\text{H}]_{\text{acc}} = 0.1$ and $\alpha T = 0.010$) in the parameter space that we have searched ($0.1 < [\text{}^4\text{He}/\text{}^1\text{H}]_{\text{acc}} < 3.0$ and $0.010 < \alpha T < 0.050$); we do not expect that a search over a more extended space will significantly improve the quality of fit for this case.

We see that the best fit is achieved in case 1 with $[\text{}^4\text{He}/\text{}^1\text{H}]_{\text{acc}} = 1$ (Fig. 1a), a value which is larger than $[\text{}^4\text{He}/\text{}^1\text{H}]_{\text{acc}}$ observed in any SEP event (Reames, Cane, & von Rosenvinge 1990). We note, however, that the fit is almost as good with the more reasonable value of $[\text{}^4\text{He}/\text{}^1\text{H}]_{\text{acc}} = 0.5$. The qualities of fit for cases 2 and 3 (where the ambient abundances are fixed, Fig. 1b and 1c) are not as good as those of case 1 (where all the abundances are allowed to vary), but the maximal values of P_{χ^2} are not low enough to allow us to reject these cases. In both of these cases the best-fitting values of $[\text{}^4\text{He}/\text{}^1\text{H}]_{\text{acc}}$ (0.1 for case 2 and 0.5 for case 3) are reasonable. The quality of fit for case 4, where the accelerated particle abundances are fixed at LPF values, is also acceptable (Fig. 1d), but it is achieved at $[\text{}^4\text{He}/\text{}^1\text{H}]_{\text{acc}} = 1$, an unacceptable value for such flares (Reames et al. 1990). Because of the rapid drop of P_{χ^2} , $[\text{}^4\text{He}/\text{}^1\text{H}]_{\text{acc}}$ cannot be reduced to acceptable values for large proton flares (0.01 to 0.1) and still obtain an

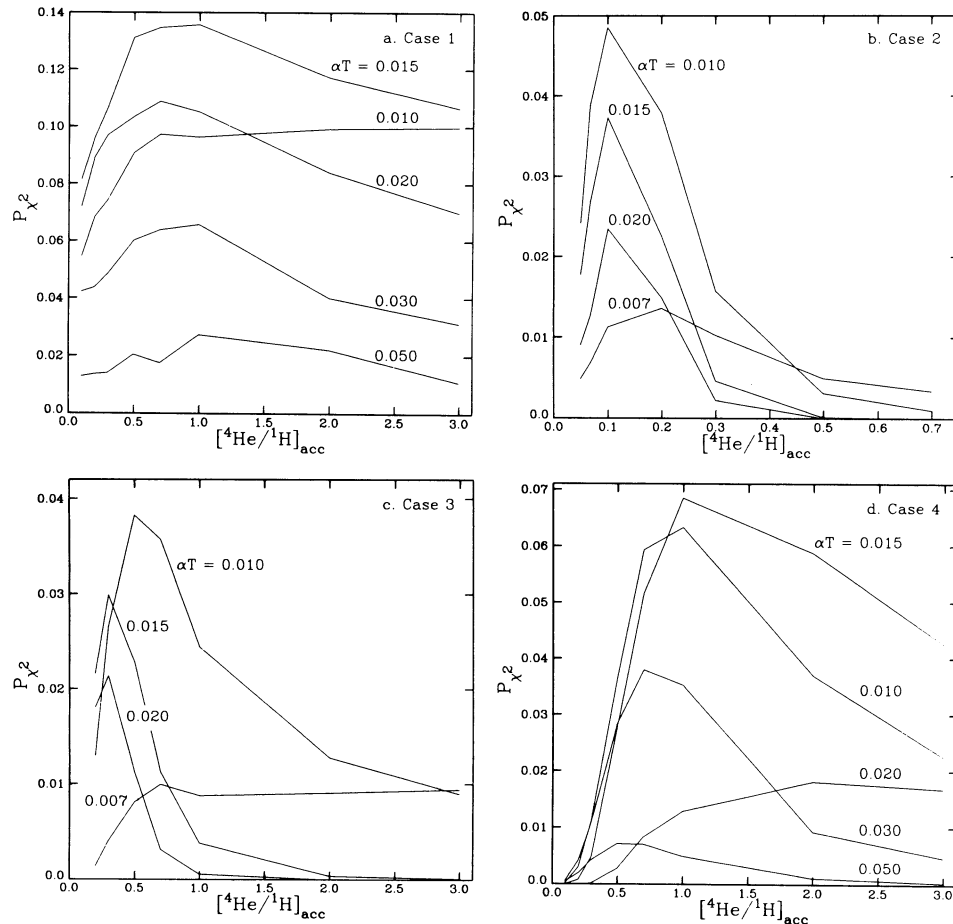


FIG. 1.—Qualities of fit P_{χ^2} as a function of $[\text{}^4\text{He}/\text{}^1\text{H}]_{\text{acc}}$ for various values of αT , the parameter which characterizes the accelerated particle spectra. (a)–(d) Cases 1–4 shown in Table 1, where the values of ν used to convert χ^2 to P_{χ^2} are given.

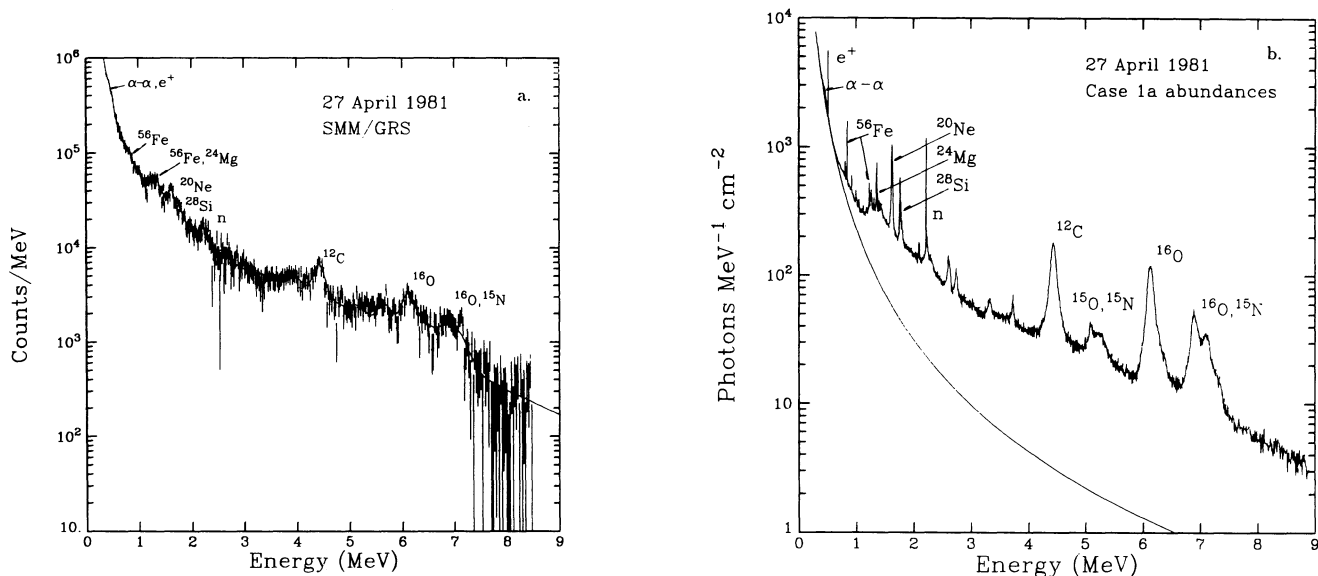


FIG. 2.—(a) Observed count spectrum of the 1981 April 27 flare fitted with the calculated spectrum for case 1 with $[^4\text{He}/^1\text{H}]_{\text{acc}} = 0.5$. (b) Corresponding calculated photon spectrum.

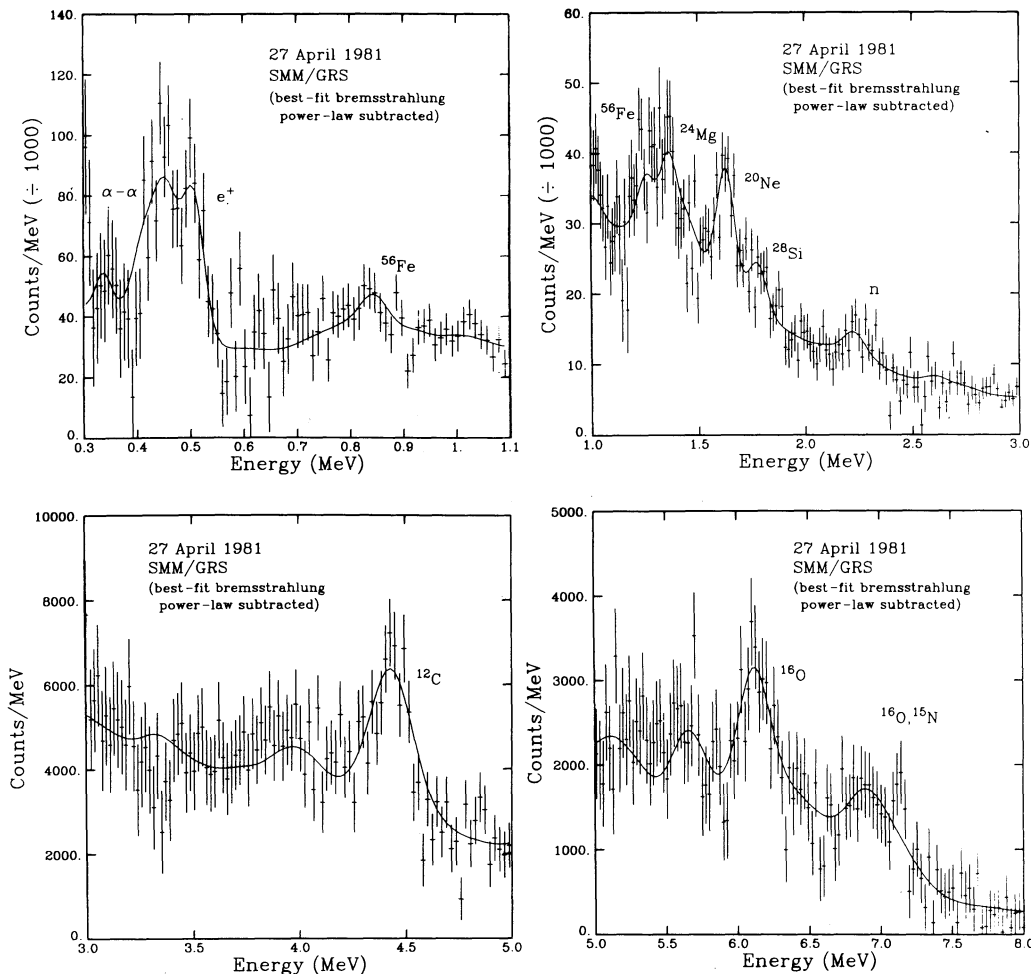


FIG. 3.—Observed and calculated count spectra for case 1

acceptable fit. This case therefore can probably be rejected. Case 5, in which both the accelerated particle and ambient abundances are fixed, can be completely rejected since the best fit that we found (Table 1) yields a very low P_{χ^2} .

Our best fit of $P_{\chi^2} = 0.14$ can be compared with that achieved ($P_{\chi^2} = 0.57$) by Murphy et al. (1990) who also fitted the same flare data. The model used in their analysis was composed of 13 narrow Gaussians representing the strongest narrow lines appearing in the observed spectrum, superposed on a continuum composed of a power law representing the electron bremsstrahlung and five broad Gaussians representing the broad nuclear lines from the inverse component. The central energies and widths of the narrow Gaussians were allowed to vary in the fitting process, whereas in the present analysis these parameters are determined theoretically. Improvement in P_{χ^2} could be obtained when some of the simplifying assumptions made in the theoretical calculations are relaxed, in particular, allowing for different kinetic energy spectra for the various species of accelerated particles, of which ^4He is, perhaps, most important.

In Figure 2a we show the observed (Murphy et al. 1990b) background-subtracted count spectrum (with 1σ error bars) from the 1981 April 27 flare together with the count spectrum (solid curve) calculated in case 1 for $[\text{}^4\text{He}/\text{}^1\text{H}]_{\text{acc}} = 0.5$. Hereafter we refer to this calculation as case 1a. The corresponding

incident photon spectrum is shown in Figure 2b, where the smooth curve represents the bremsstrahlung fluence. The differences between the line spectra in the two panels show the degrading effects of the SMM NaI spectrometer. Clearly, much more information on solar abundances will be obtained by future observations with high-resolution Ge detectors which will be able to identify the individual lines seen in the calculated spectrum of Figure 2b.

In Figures 3–8, we show the same data fitted with the calculated spectra for cases 1, 1a, 2, 3, 4, and 5. In these figures, the best-fitting bremsstrahlung power laws are subtracted from both the data and the calculated spectra. The nuclei responsible for the various lines are indicated, and n and e^+ denote the neutron capture and positron annihilation lines. For the full-fit cases (Figs. 3 and 4), essentially all line features are well fitted. In Figures 5 and 6 (for which the ambient abundances are photospheric or coronal) the narrow line of Ne (1.634 MeV) is not as well fitted as in Figures 3 and 4. In addition, in Figure 5, for which $[\text{}^4\text{He}/\text{}^1\text{H}]_{\text{acc}}$ is relatively small ($[\text{}^4\text{He}/\text{}^1\text{H}]_{\text{acc}} = 0.1$), a line feature at ~ 1.02 MeV is not as well fitted as in Figure 3. An important contribution to the emission in this energy region comes from the reactions $^{56}\text{Fe}(\alpha, n\gamma_{0.999})^{59}\text{Ni}$, $^{56}\text{Fe}(\alpha, 2n\gamma_{1.005})^{58}\text{Ni}$, and $^{56}\text{Fe}(\alpha, pn\gamma_{1.05})^{58}\text{Co}$ (Seamster et al. 1984). Since these lines are produced by α -particles but not by protons, the feature at ~ 1.02 MeV can be

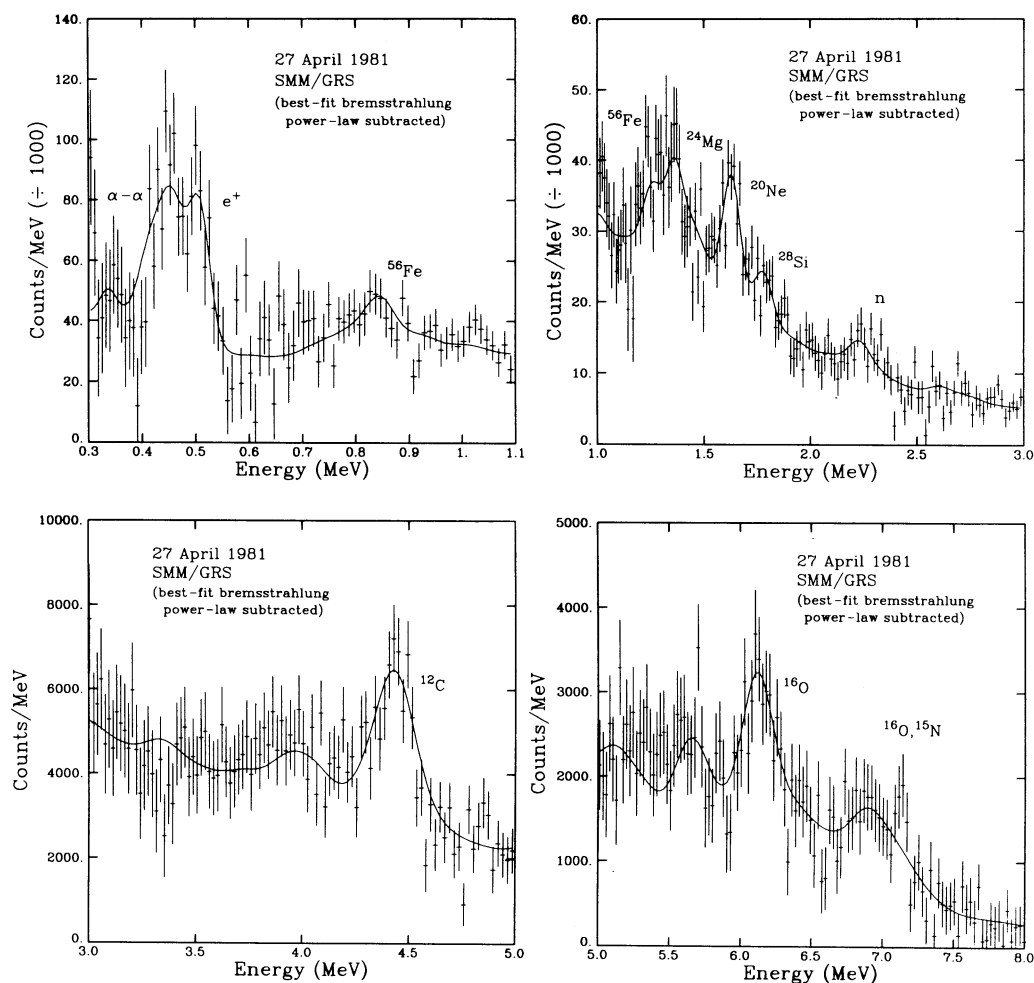


FIG. 4.—Observed and calculated count spectra for case 1a

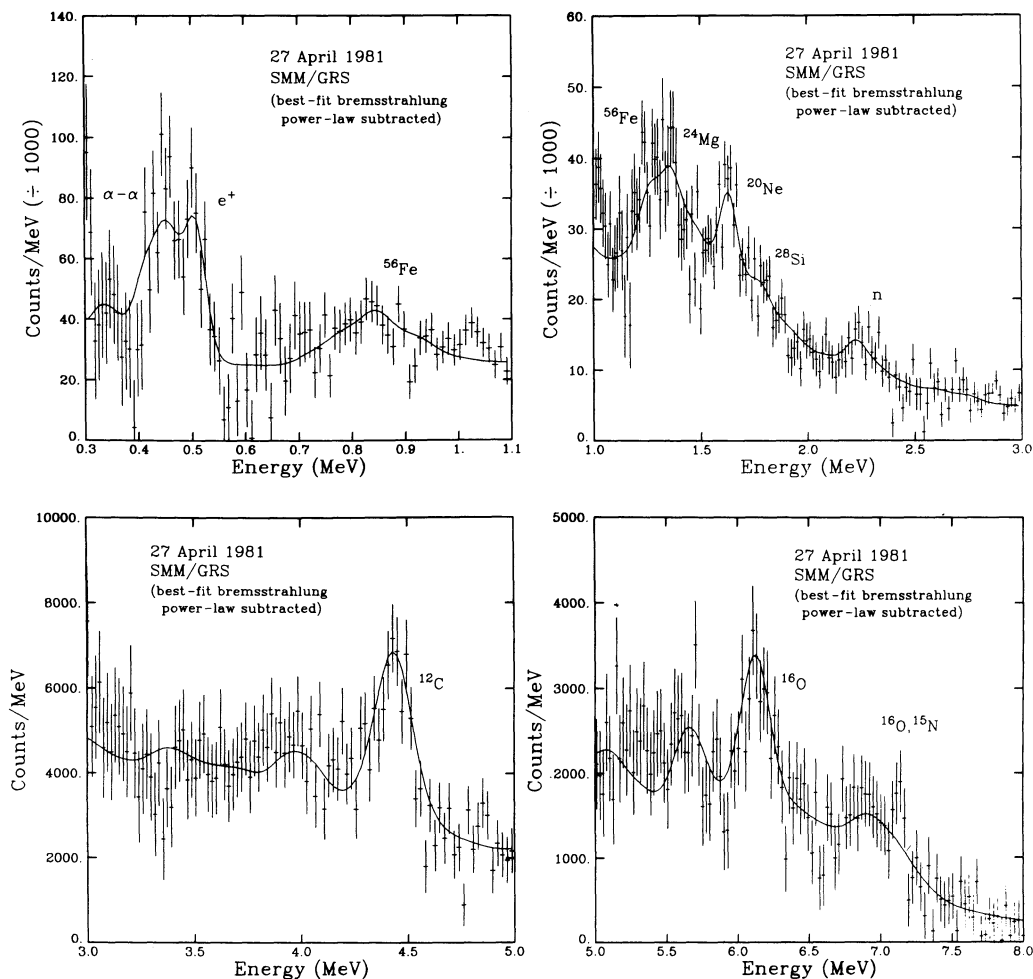


FIG. 5.—Observed and calculated count spectra for case 2

better fitted when $[\text{He}/\text{H}]_{\text{acc}}$ is high. The fit is particularly bad in Figure 8, especially in the 1–2 MeV region. As indicated above, this case can be completely rejected.

The derived best-fitting ambient abundances for cases 1, 1a, and 4 are given in Table 2, where they are compared with photospheric abundances (Anders & Grevesse 1989) and coronal abundances (Breneman & Stone 1985; Anders & Gre-

vesse 1989). The best-fitting accelerated particle abundances for cases 1, 1a, 2, and 3 are given in Table 3, where they are compared with average accelerated particle abundances observed in large proton flares and in ^3He -rich flares. The LPF data are from Breneman & Stone (1985), except $^3\text{He}/^4\text{He}$, which is from McGuire, von Roseninge, & McDonald (1986); the ^3He -rich flare data are from Reames et al. (1990). The

TABLE 2
 AMBIENT MEDIUM ABUNDANCES COMPARED WITH PHOTOSPHERIC ABUNDANCES^a
 AND CORONAL ABUNDANCES^b

Element	Case 1	Case 1a ^c	Case 4	Photospheric Abundances	Coronal Abundances
^4He	82.5 ± 11.4	108 ± 15	82.4 ± 12.1	269^{+23}_{-21}	174^{+26}_{-23}
C	1.00 ± 0.20	1.00 ± 0.19	1.00 ± 0.15	$1.00^{+0.10}_{-0.09}$	$1.00^{+0.11}_{-0.10}$
N	0.13 ± 0.51	0.23 ± 0.48	0.43 ± 0.44	$0.31^{+0.03}_{-0.03}$	$0.30^{+0.02}_{-0.02}$
O	2.40 ± 0.27	2.37 ± 0.27	2.32 ± 0.22	$2.34^{+0.20}_{-0.18}$	$2.42^{+0.15}_{-0.14}$
Ne	0.99 ± 0.16	0.91 ± 0.15	1.07 ± 0.11	$0.34^{+0.09}_{-0.07}$	$0.33^{+0.04}_{-0.03}$
Mg	0.46 ± 0.16	0.35 ± 0.13	0.73 ± 0.13	$0.105^{+0.013}_{-0.011}$	$0.46^{+0.03}_{-0.03}$
Si	0.63 ± 0.17	0.52 ± 0.15	0.72 ± 0.12	$0.098^{+0.012}_{-0.011}$	0.43
Fe	0.42 ± 0.13	0.37 ± 0.12	0.90 ± 0.07	$0.130^{+0.009}_{-0.009}$	$0.54^{+0.07}_{-0.06}$

^a Anders & Grevesse 1989.

^b Breneman & Stone 1985.

^c Case 1 with $[\text{He}/\text{H}]_{\text{acc}} = 0.5$.

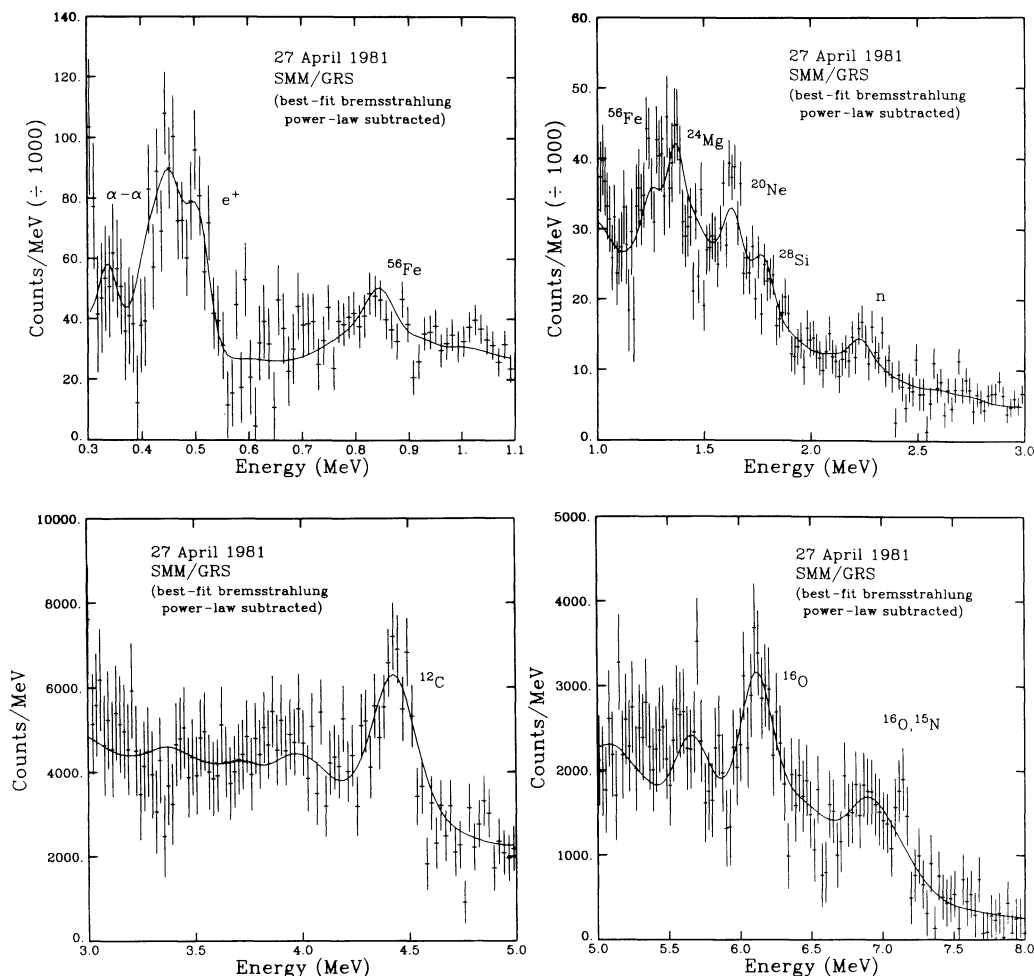


FIG. 6.—Observed and calculated count spectra for case 3

best-fitting values for the normalizations $[n_c/n_H]N_p$ and N_C , the incident narrow 2.223 and 0.511 MeV line fluences, the incident bremsstrahlung fluence above 300 keV, and the bremsstrahlung power-law spectral index s are shown in Table 4 for cases 1, 1a, 2, 3, and 4. The uncertainties of all the gamma-ray-derived results are estimated using $\Delta\chi^2 = 1$.

Considering first the ambient abundances, we see in Table 2 that in cases 1 and 1a, Mg/C, Si/C, and Fe/C are enhanced

relative to the photosphere but not relative to the corona, while Ne/C is enhanced relative to both the photosphere and the corona. We note that the photospheric Ne/C has not been directly measured; the value in Table 2 is actually the coronal value which is consistent with the recent observations of Feldman & Widing (1990) of impulsive flare material which they show to be similar to photospheric material. In addition, for cases 1 and 1a, He/C is suppressed relative to both the

TABLE 3
ACCELERATED PARTICLE ABUNDANCES COMPARED WITH LARGE PROTON FLARE ABUNDANCES^a
AND ³He-RICH FLARE ABUNDANCES^b

Element	Case 1	Case 1a ^c	Case 2	Case 3	Large Proton Flare (LPF)	³ He-rich Flare
³ He/ ⁴ He	0.28 ± 0.38	0.50 ± 0.39	1.32 ± 0.34	0.03 ± 0.01	<0.05	>0.1
C	1.00 ± 1.65	1.00 ± 0.96	1.00 ± 0.29	1.00 ± 0.27	1.00 ± 0.10	1.00
N	7.54 ± 5.50	4.73 ± 3.39	3.60 ± 1.18	3.11 ± 1.09	0.29 ± 0.02	0.2–0.8
O	1.69 ± 2.75	2.00 ± 1.59	2.78 ± 0.54	2.01 ± 0.52	2.30 ± 0.06	1–6
Ne	0.26 ± 2.36	<1.47	0.71 ± 0.39	1.28 ± 0.35	0.33 ± 0.03	0.3–5
Mg	5.67 ± 2.22	4.94 ± 1.26	3.73 ± 0.39	2.05 ± 0.37	0.45 ± 0.02	0.5–4
Si	<2.97	0.90 ± 1.75	2.80 ± 0.66	1.42 ± 0.61	0.37	0.5–3
Fe	10.3 ± 2.44	6.35 ± 1.46	4.28 ± 0.42	3.10 ± 0.40	0.35 ± 0.04	1–10

^a Breneman & Stone 1985.^b Reames et al. 1990.^c Case 1 with $[^4\text{He}/^1\text{H}]_{\text{acc}} = 0.5$.

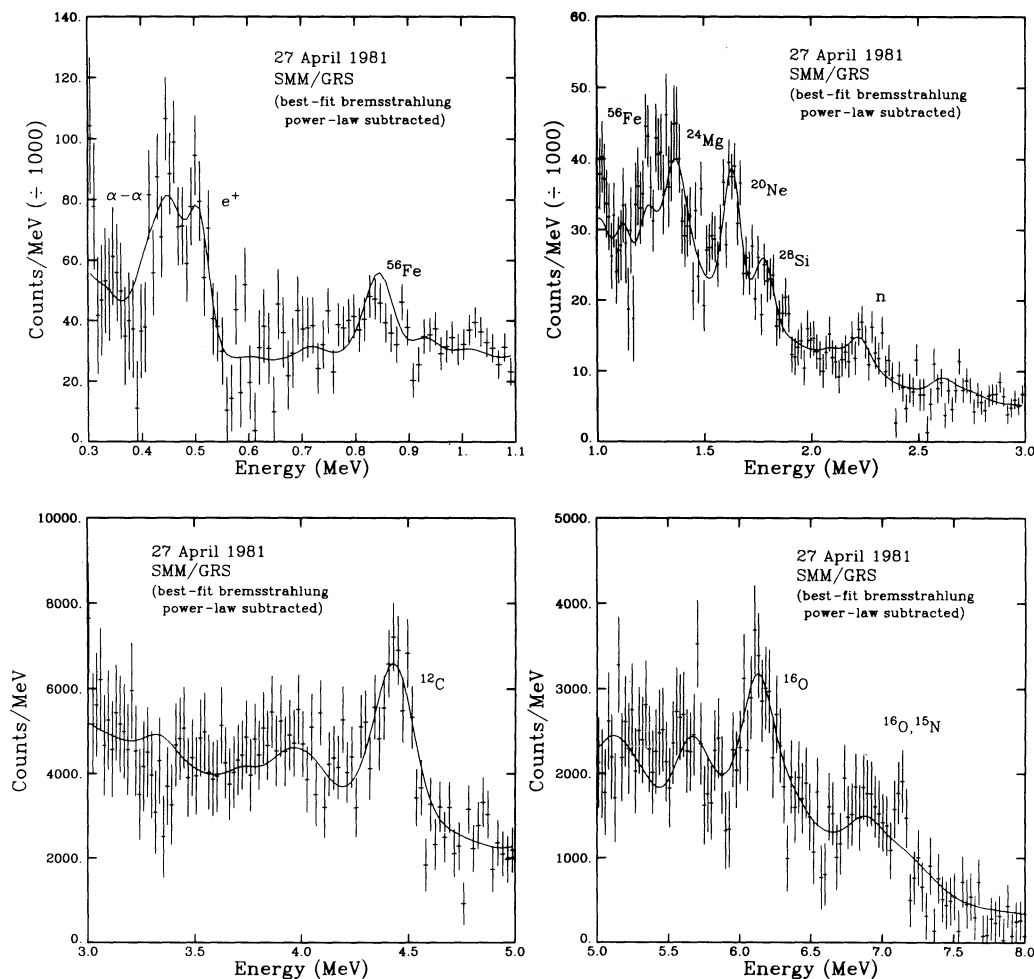


FIG. 7.—Observed and calculated count spectra for case 4

photosphere and the corona. These differences, derived for cases 1 and 1a, should be contrasted with cases 2 and 3, for which the ambient abundances are photospheric or coronal by definition. Since, as discussed above, the qualities of fit for cases 2 and 3 are not much worse than those for cases 1 and 1a, it is possible that the composition of the ambient medium is either photospheric or coronal.

3. COMPARISON WITH SOLAR ENERGETIC PARTICLE OBSERVATIONS

We proceed now to compare the derived accelerated particle abundances with SEP observations. The case in which the accelerated particle abundances are fixed at LPF values (case

4) provides a fit with $P_{\chi^2} = 0.069$, but this fit requires $[\text{He}/\text{H}]_{\text{acc}} = 1.0$ (Fig. 1d). As we have discussed above, this $[\text{He}/\text{H}]_{\text{acc}}$ is much larger than the values of $[\text{He}/\text{H}]_{\text{acc}}$ observed in large proton flares for which $[\text{He}/\text{H}]_{\text{acc}}$ ranges from about 0.01 to 0.1 (Reames et al. 1990). For such low values of $[\text{He}/\text{H}]_{\text{acc}}$, Figure 1d shows that the fit is unacceptable, implying that the composition of the accelerated particles is probably different from that of large proton flares.

We see in Table 3 that, in general, the derived abundances of the heavy accelerated particles (in particular Fe) are enhanced relative to the LPF values and resemble more closely ^3He -rich flare abundances. The derived accelerated particle abundances for cases 1a and 2 are plotted in Figures 9 and 10, along with

TABLE 4
TOTAL ACCELERATED PROTON AND CARBON NUMBERS, INCIDENT 2.223 AND 0.511 MeV FLUENCES,
AND BREMSSTRAHLUNG SPECTRAL INDEX AND FLUENCE ABOVE 0.3 MeV

Parameter	Case 1	Case 1a ^a	Case 2	Case 3	Case 4
$10^{-28} [n_{\text{C}}/n_{\text{H}}] N_p$	5.54 ± 1.09	8.18 ± 1.52	7.56 ± 0.47	3.36 ± 0.21	5.19 ± 0.76
$10^{-28} N_{\text{C}}$	7.67 ± 12.7	12.6 ± 12.2	12.1 ± 3.6	13.1 ± 3.5	15.4 ± 5.4
$\phi_{2.223}$ (photons cm^{-2})	1.46 ± 2.10	2.93 ± 2.04	3.75 ± 2.03	2.74 ± 2.05	2.08 ± 1.95
$\phi_{0.511}$ (photons cm^{-2})	7.33 ± 1.90	7.30 ± 1.90	7.09 ± 1.67	5.89 ± 1.71	6.76 ± 1.89
s	2.90 ± 0.02	2.90 ± 0.02	2.85 ± 0.02	2.87 ± 0.01	2.87 ± 0.01
$10^{-3} \phi_{\text{B}} (>0.3 \text{ MeV})$ (photons cm^{-2})	1.23 ± 0.69	1.24 ± 0.68	1.26 ± 0.66	1.24 ± 0.70	1.25 ± 0.69

^a Case 1 with $[\text{He}/\text{H}]_{\text{acc}} = 0.5$.

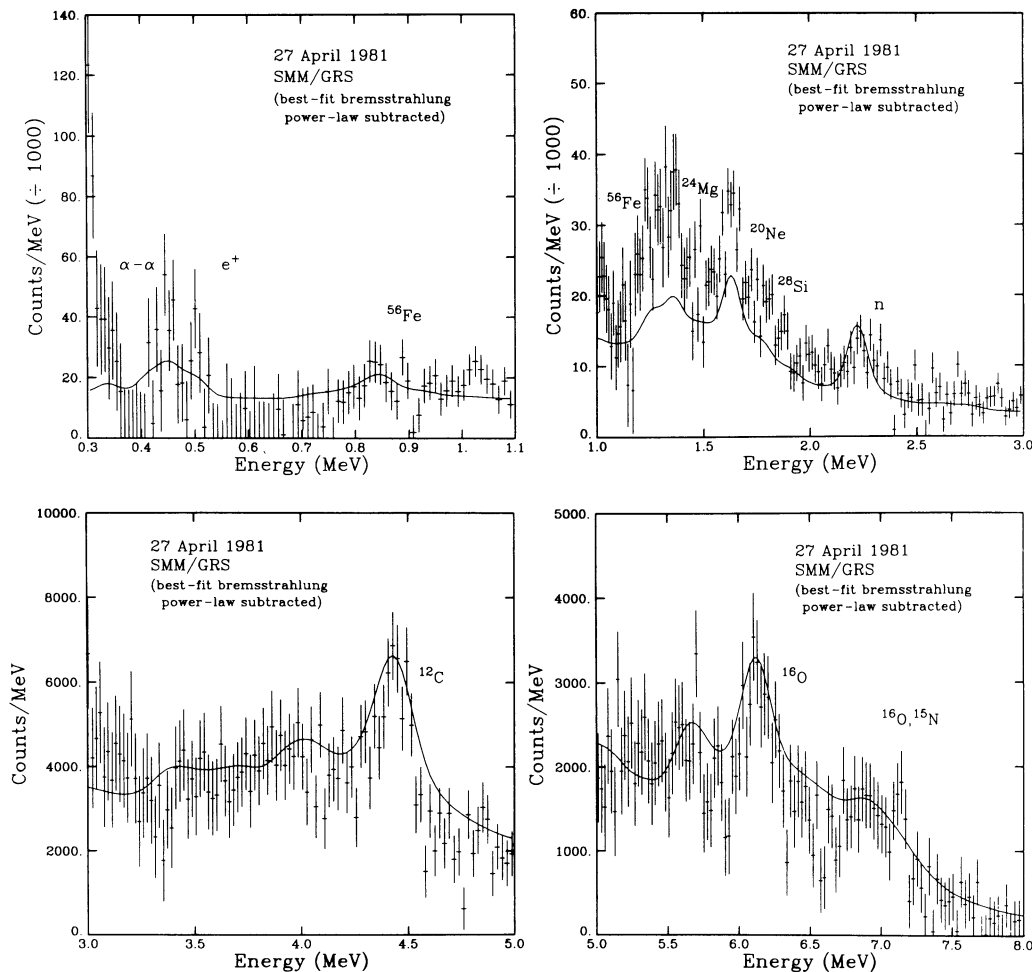


FIG. 8.—Observed and calculated count spectra for case 5

SEP data from Reames et al. (1990). In Figure 9 the SEP data show the bimodal distributions of Fe/C and Fe/O, which support the existence of the two classes of SEP events. The blackened areas represent ^3He -rich events, which, as can be seen, correspond to high values of Fe/C and Fe/O. The events with low Fe/C and Fe/O are large proton events. We see that the gamma-ray-derived abundances, in particular those for case 2 in which the ambient abundances are fixed and the uncertainties are smaller, are more consistent with the ^3He -rich SEP abundances than with large proton flare abundances. In Figure 10 the open circles show O/C, Ne/C, Mg/C, and Si/C as a function of Fe/C for a number of SEP events. The open squares are the LPF values. The closed circles and squares show derived values of these ratios for cases 1a and 2, respectively. We see that for the SEP data there is a strong correlation of Ne/C, Mg/C, and Si/C with Fe/C, indicating that these abundance ratios are also enhanced in ^3He -rich flares. Furthermore, the values of Ne/C, Mg/C, and Si/C implied by the gamma-ray data in case 2 agree with the enhanced values of these ratios found in ^3He -rich events, again showing that the composition of the accelerated particles which produce the gamma rays is more consistent with that of ^3He -rich flares than with that of large proton flares.

We return now to the question of $[\text{}^4\text{He}/\text{}^1\text{H}]_{\text{acc}}$, and we also consider $[\text{}^3\text{He}/\text{}^4\text{He}]_{\text{acc}}$. We have values of $[\text{}^4\text{He}/\text{}^1\text{H}]_{\text{acc}}$ of 1.0, 0.5, 0.1, and 0.5 for cases 1, 1a, 2, and 3, respectively. (Cases 4

and 5 were found to be unacceptable.) These results indicate that $[\text{}^4\text{He}/\text{}^1\text{H}]_{\text{acc}}$ is probably larger than 0.1. An independent argument leading to a similar result follows from the values given in Table 5. Here we show the dependence of the derived ambient $^4\text{He}/\text{C}$ on $[\text{}^4\text{He}/\text{}^1\text{H}]_{\text{acc}}$ for case 1, where for each value of $[\text{}^4\text{He}/\text{}^1\text{H}]_{\text{acc}}$ all of the other parameters are varied to maximize P_{χ^2} . We see that $^4\text{He}/\text{C}$ decreases as $[\text{}^4\text{He}/\text{}^1\text{H}]_{\text{acc}}$ increases. This inverse dependency arises because of the fixed observed ratio of the strengths of the ^7Li - ^7Be lines (due to α -particle interactions with ambient He) to the strengths of the other narrow lines (due to proton and α -particle interaction with ambient heavy nuclei). Comparing the derived $^4\text{He}/\text{C}$ with the photospheric value of 269^{+23}_{-21} (Anders & Grevesse 1989), we again conclude that $[\text{}^4\text{He}/\text{}^1\text{H}]_{\text{acc}}$ is probably not much smaller than 0.1, since it is unlikely that the He/C ratio in

TABLE 5
AMBIENT $^4\text{He}/\text{C}$ AS A FUNCTION
OF $[\text{}^4\text{He}/\text{}^1\text{H}]_{\text{acc}}$ FOR CASE 1

$[\text{}^4\text{He}/\text{}^1\text{H}]_{\text{acc}}$	$^4\text{He}/\text{C}$
3.0	66.5 ± 8.8
2.0	69.8 ± 9.4
1.0	82.5 ± 11.4
0.2	194 ± 28
0.1	329 ± 48

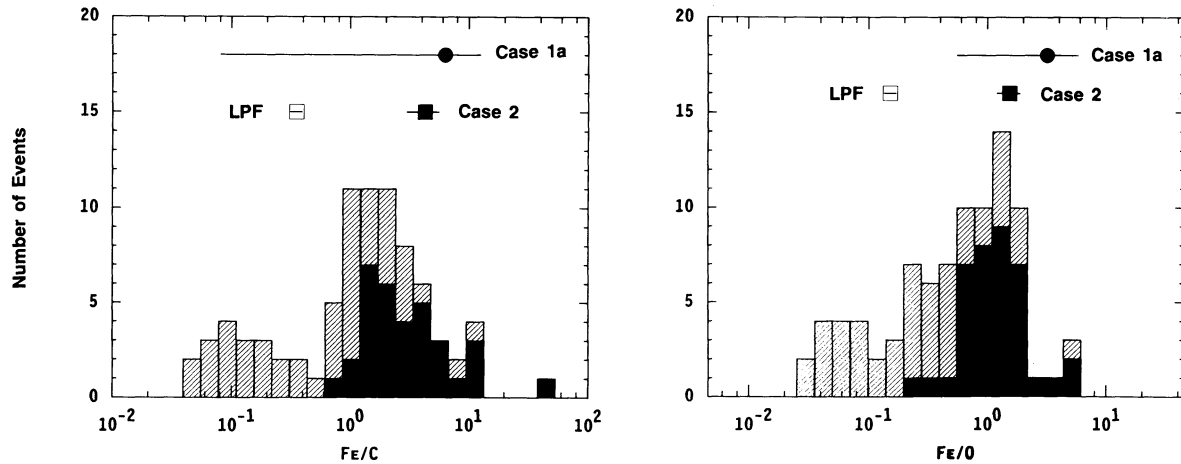


FIG. 9.—Histograms of the distributions of Fe/C and Fe/O in SEP events with the ^3He -rich subset blackened (from Reames et al. 1990). The gamma-ray results for the accelerated particles (from Table 3, after propagation of the errors) are also shown for cases 1a and 2. The large proton flare abundances of Table 3 are shown by open squares.

the ambient gas significantly exceeds the photospheric value. Since, as mentioned above, $[\text{}^4\text{He}/\text{}^1\text{H}]_{\text{acc}}$ in large proton events is typically less than 0.1, while in ^3He -rich events $[\text{}^4\text{He}/\text{}^1\text{H}]_{\text{acc}}$ tends to be larger (Ramaty et al. 1980; Reames et al. 1990), this result is another indication for the similarity of the accelerated particles which produce the gamma rays and SEP in ^3He -rich events. As for $[\text{}^3\text{He}/\text{}^4\text{He}]_{\text{acc}}$, the derived values of this ratio (Table 3) are also generally indicative of an enrichment of ^3He relative to ^4He , although the uncertainty in this derivation is quite large since ^3He interactions produce just one weak gamma-ray line, at 3.561 MeV from ^6Li (see Ramaty, Kozlovsky, & Lingenfelter 1979).

4. SUMMARY

Using gamma-ray observations of the 1981 April 27 flare, we have derived elemental abundances of both the ambient gas and the accelerated particles which interact with this gas to produce the gamma rays. The derived ambient gas abundances pertain to the gamma-ray production site whose location is not known. For impulsive flares, this site is probably in the chromosphere, but for an extended flare such as the 1981 April 27 flare, significant gamma-ray production could take place in the corona if the coronal density exceeds $5 \times 10^{11} \text{ cm}^{-3}$. We found that the case in which the composition of the ambient

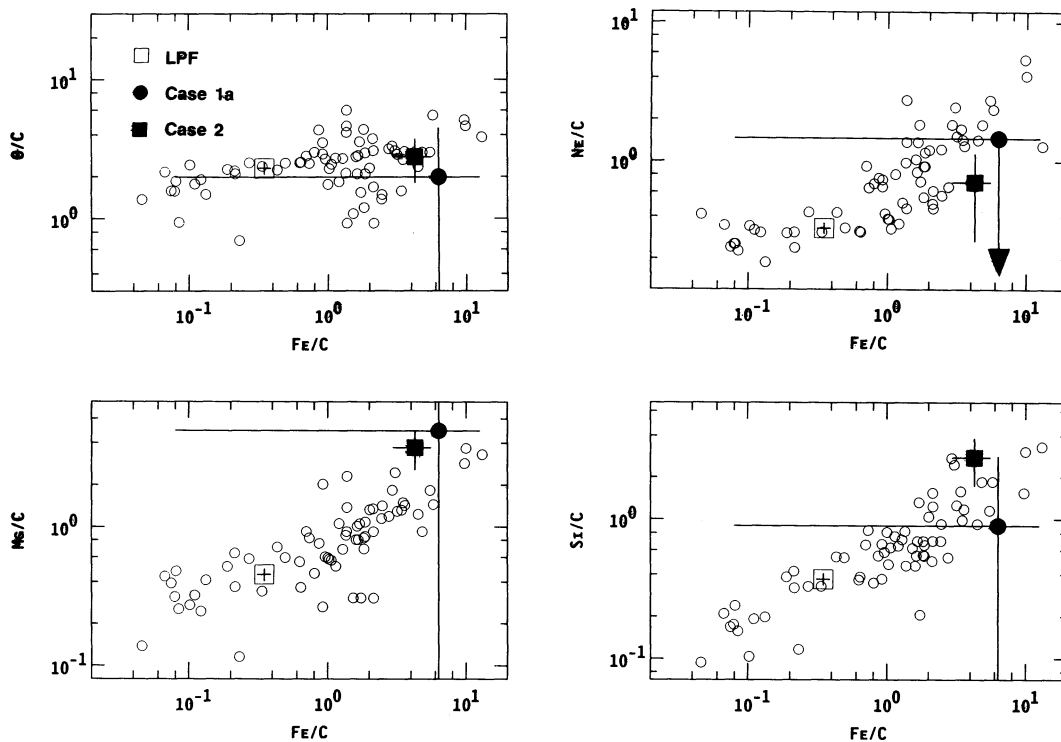


FIG. 10.—Abundance ratios as a function of Fe/C. The open circles are from Reames et al. (1990), and the open squares are the large proton flare values from Table 3. The gamma-ray results for case 1a are shown as closed circles and for case 2 are closed squares.

gas is photospheric and the composition of the accelerated particles is fixed at large proton flare (LPF) values can be clearly rejected. Furthermore, the case in which the accelerated particle composition is fixed at LPF values but the ambient gas is allowed to vary can probably also be rejected. The best fit to the data (acceptable at the 13% confidence level) is obtained when both the ambient and the accelerated particle abundances are allowed to vary. This full fit suggests that Mg/C, Si/C, and Fe/C in the ambient gas are enhanced relative to the corresponding ratios in the photosphere but not relative to those in the corona, and that the ambient Ne/C is enhanced relative to the coronal value. While the best fit to the data is obtained with ambient abundances which differ from both photospheric and coronal abundances, the cases in which the abundances of the ambient gas are fixed at photospheric or coronal values are also acceptable but only at the 5% and 4% levels, respectively.

The cases in which the ambient abundances are photospheric or coronal yield accelerated particle abundances (including $[^4\text{He}/^1\text{H}]_{\text{acc}}$) which imply that this particle popu-

lation resembles the solar energetic particles observed from ^3He -rich flares rather than the composition of the particles observed from large proton flares. The accelerated particle abundances in the full-fit case are not well determined, but, as we have pointed out above, the accelerated particle abundances are in any case different from LPF values. Since the accelerated particles which produce the gamma rays are most likely accelerated in closed flare loops (Ramaty & Murphy 1987), our results provide support to the suggestion (Luhn et al. 1987; Lin 1987) that the particles observed in ^3He -rich events are accelerated from hot flare plasma. However, it is not known whether the energetic particles observed from ^3He -rich flares are accelerated in closed loops and subsequently escape from the loops, or whether they are accelerated from hot flare plasma on open field lines.

We wish to acknowledge D. J. Forrest for useful discussions and H. V. Cane for comments. The calculations were performed on the NRL Central Computing Facility Cray X-MP computer.

REFERENCES

- Anders, E., & Grevesse, N. 1989, *Geochim. Cosmochim. Acta*, 53, 197
 Breneman, H. H., & Stone, E. C. 1985, *ApJ*, 299, L57
 Cane, H. V., McGuire, R. E., & von Rosenvinge, T. T. 1986, *ApJ*, 310, 448
 Crannell, C. J., Joyce, G., Ramaty, R., & Wertz, C. 1976, *ApJ*, 210, 52
 Feldman, U., & Widing, K. G. 1990, *ApJ*, 363, 292
 Forman, M. A., Ramaty, R., & Zweibel, E. G. 1986, in *The Physics of the Sun*, Vol. 2, ed. P. A. Sturrock et al. (Dordrecht: Reidel), 249
 Forrest, D. J. 1983, in *Positron Electron Pairs in Astrophysics*, ed. M. L. Burns, A. K. Harding, & R. Ramaty (New York: AIP), 3
 Hua, X. M., Ramaty, R., & Lingenfelter, R. E. 1989, *ApJ*, 341, 516
 Lin, R. P. 1987, *Rev. Geophys.*, 25, 676
 Luhn, A., Klecker, B., Hovestadt, D., & Möbius, E. 1987, *ApJ*, 317, 951
 McGuire, R. E., von Rosenvinge, T. T., & McDonald, F. B. 1986, *ApJ*, 301, 938
 Meyer, J. P. 1985, *ApJS*, 57, 151
 Murphy, R. J. 1985, Ph.D. thesis, University of Maryland
 Murphy, R. J., Forrest, D. J., Ramaty, R., & Kozlovsky, B. 1985a, *Proc. 19th Internat. Cosmic Ray Conf. (La Jolla)*, 4, 253
 Murphy, R. J., Hua, X. M., Kozlovsky, B., & Ramaty, R. 1990a, *ApJ*, 351, 299
 Murphy, R. J., & Ramaty, R. 1984, *Adv. Space Res.*, 4, 127
 Murphy, R. J., Ramaty, R., Forrest, D. J., & Kozlovsky, B. 1985b, *Proc. 19th Internat. Cosmic Ray Conf. (La Jolla)*, 4, 249
 Murphy, R. J., Share, G. H., Letaw, J. R., & Forrest, D. J. 1990b, *ApJ*, 358, 290
 Ramaty, R., et al. 1980, in *Solar Flares*, ed. P. A. Sturrock (Boulder: Colorado Assoc. University Press), 117
 Ramaty, R., Kozlovsky, B., & Lingenfelter, R. E. 1975, *Space Sci. Rev.*, 18, 341
 ———. 1979, *ApJS*, 40, 487
 Ramaty, R., Miller, J. A., Hua, X. M., & Lingenfelter, R. E. 1990, *ApJS*, 73, 199
 Ramaty, R., & Murphy, R. J. 1987, *Space Sci. Rev.*, 45, 213
 Reames, D. V. 1990, *ApJS*, 73, 235
 Reames, D. V., Cane, H. V., & von Rosenvinge, T. T. 1990, *ApJ*, 357, 259
 Seamster, A. G., Norman, E. B., Leach, D. D., & Bodansky, D. 1984, *Phys. Rev. C*, 29, 394
 Suri, A. N., Chupp, E. L., Forrest, D. J., & Reppin, C. 1975, *Solar Phys.*, 43, 414
 Trombka, J. I., & Schmadebeck, R. L. 1968, NASA SP-3044